



cambridge.org/mrf

Ankita Malhotra¹  and Ananjan Basu²

¹Electronics and Telecommunications Department, R.G.I.T, Mumbai, India and ²Centre for Applied Research in Electronics, IIT, Delhi, India

Research Paper

Cite this article: Malhotra A, Basu A (2023). Broadband frequency reconfigurable printed transceivers for microwave imaging systems. *International Journal of Microwave and Wireless Technologies* **15**, 1130–1138. <https://doi.org/10.1017/S1759078722001155>

Received: 9 April 2022
Revised: 25 September 2022
Accepted: 26 September 2022

Key words:

Antenna; imaging; microwave; reconfigurable; 2D scanning

Author for correspondence:

Ankita Malhotra,
E-mail: ankitakec52224@gmail.com

Abstract

In this paper, we propose a novel method for obtaining wideband spectral information of the target in microwave imaging systems by using broadband frequency reconfigurable printed transceivers. The proposed transceiver is composed of two embedded stacked microstrip antenna configurations operating in C-band (5.5–8.5 GHz) and X-band (8.5–11.5 GHz) with each having 3 GHz bandwidth. The transceiver switches between the two configurations (and thus frequency bands) using PIN diodes and collects response of the antenna in the presence of the target, in both the operating bands. This information is then combined to obtain wideband spectral information of the target from 5.5 to 11.5 GHz to achieve improved image reconstruction. The proposed reconfigurable transceiver has advantage over traditional broadband transceivers (those have slots/meandering at ground plane to achieve wideband response) that it has unidirectional radiation patterns throughout its band of operation. Hence the imaging system is implemented without the absorbers. This keeps the system compact and inconspicuous when installed for security applications. Here, a bistatic system is employed with two-dimensional target scanning performed in a real outdoor environment.

Introduction

Microwave imaging is an emerging tool for non-destructive testing of objects under interrogation. Several researchers have explored its potential in various applications. The non-ionizing property of microwaves and their capability to map the dielectric contrast of the investigation domain make them suitable for biomedical applications such as head imaging to detect brain tumor [1–3], and early-stage breast cancer detection [4–8]. Similarly, microwave imaging has been used to detect dielectric objects [9, 10], where efforts have been made to reconstruct the three-dimensional (3D) image of microwave absorber sample [9] and image reconstruction of different dielectric materials [10]. Furthermore, microwave imaging is widely used for security applications to detect and reconstruct the image of suspicious hidden targets and through-the-wall imaging utilizing their capability to penetrate. Typically horn antennas (large setups) are used for improved beam forming and the imaging systems are kept in an anechoic chamber or with absorbers [11–13]. The hidden target detection is presented in [11], beneath three-layer body model, while images of large metallic objects have been obtained in [12] by applying factorization method. Furthermore, near-field microwave imaging using resonately loaded apertures is carried out in [13], where mostly the target detection is achieved. A microwave camera for hidden target detection presented in [14] can be quite useful for baggage scanning to find suspicious metallic objects inside the bag. However, here a large reflector is used to allow most of the scattered waves reach the receivers, which makes the system bulky and difficult to use practically.

Moreover, research is carried out for improved resolution in microwave imaging by using ultra-wideband (UWB) transceivers to capture more spectral information of the target. Typically, they are used for through-the-wall imaging [15] and for the imaging of inclusions in dielectric cylinders/spheres for medical application [16]. In through-the-wall human detection, using UWB radar [17] the presence and displacement of human behind the wall is detected. Detection of partially occluded objects is presented in [18] using UWB transceivers. In [19] through-the-wall object detection is carried out in the X-band, while in [20] through-the-wall object detection is carried out in the S-band with improved resolution using a two-step inverse scattering technique. However, in [17–20], the main focus is on target detection rather than image reconstruction.

A multistatic UWB microwave imaging system is presented in [21] where the antenna is backed by a metallic reflector (increasing its size) to make it unidirectional, where regular planar shapes have been used as target objects and the image quality is still average. In [22] a microwave imaging system using an optimized number of transceivers on demand, based on analytical equation, is proposed, where regular-shaped metallic targets are used for testing. Moreover, the imaging setup is placed in an anechoic chamber to avoid noise in the resultant reconstructed

images. The above discussed microwave imaging systems have bulky setups placed in either an anechoic chamber/with absorbers or with reflectors for their operation, to avoid backside clutter and did not employ irregular-shaped targets in the setup. The use of absorbers or reflectors restricts easy installation of the system in a real outdoor environment, especially if it needs to be compact and inconspicuous for security purposes. However use of planar and printed transceiver design with uniform ground makes it easily integrable with other circuits and easy to deploy on planar region-like wall of a scanning chamber for practical implementation. In our previous work [23] a microwave imaging system with miniaturized printed transceivers has been presented with target images obtained using X-band transceiver and also using C-band transceiver. The preliminary work of combining spectral information using simple image matrix addition obtained in different bands is also presented.

Here, we propose a planar-printed broadband reconfigurable microwave imaging system, which is compact and utilizes a novel method of obtaining wideband spectral information of the target. The transceiver has unidirectional radiation patterns throughout its wideband of operation and thus the backside clutter is rejected without the use of anechoic chamber/absorbers. The proposed reconfigurable antenna/transceiver has two states of operation in which it switches between C- and X-band regions. In C-band the transceiver covers 3 GHz bandwidth from 5.5 to 8.5 GHz and in X-band also the transceiver covers 3 GHz bandwidth from 8.5 to 11.5 GHz. The transceiver’s response obtained in both the frequency bands is then combined effectively in the frequency domain to obtain an equivalent wideband response from 5.5 to 11.5 GHz. This wideband spectral information of the target is then processed using the SAR algorithm and it gives improved image reconstruction as compared to those obtained in individual bands (X and C). The proposed work mainly focuses on the lower-frequency region of microwave band to achieve optimum range sensitivity (as per radar range detection [24]) for target detection and imaging even in an open environment, which is not the case with higher frequencies such as millimeter-wave band. Here two-dimensional (2D) distributed target scanning is implemented and microwave imaging of real-life non-planar and irregular-shaped objects is carried out in far-field. Successful target detection and improved image reconstruction is achieved.

Proposed transceiver design

The proposed broadband reconfigurable transceiver antenna comprises of two stacked configurations fabricated on a single substrate, operating in a switched mode using two pin diodes. The design is

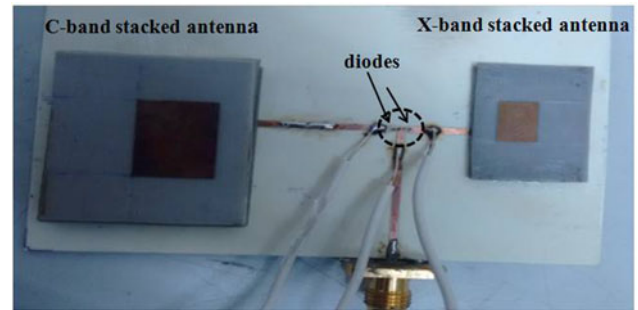


Fig. 2. Fabricated transceiver circuit.

shown in Fig. 1. When diode 1 is switched ON, the antenna operates in the C-band region with 3 GHz bandwidth from 5.5 to 8.5 GHz. When diode 2 is switched ON, the antenna operates in the X-band region with 3 GHz bandwidth from 8.5 to 11.5 GHz. The peak measured gain in C-band is 8 dBi while in X-band it is 7.7 dBi. The common 50 Ω feed line is connected to both the stacked configurations through a switch (pin-diode) for each. A regulated DC voltage supply can be connected to each diode, with the positive terminal connected to diode’s anode and the negative terminal connected to common feed line to make it a common ground. In the experiments, a potentiometer connected with DC batteries, with its common pin connected to common ground, is used. This arrangement makes the system flexible to be applicable in the imaging setup. The fabricated circuit is shown in Fig. 2 and the microwave imaging setup is demonstrated in Fig. 3. The separation between two antennas is such that $s > \lambda/4$ (larger λ) and $s \neq n\lambda$, so that their radiation patterns do not interfere with each other ($s = 4.5$ cm). In the fabricated transceiver, $l_1 = 1.1$ cm, while $l_2 = 3.1$ cm. The transceivers are designed such that their combined response in the frequency domain is a continuous wideband response. Response of the reconfigurable antenna for both the states is shown in Figs 4(a) and 4(b), respective gains are depicted in Fig. 5, and radiation patterns at different frequencies are shown in Fig. 6. Design parameters of the X-band antenna [25] and C-band antenna are listed in Tables 1 and 2, respectively. Here W_1, L_1 represent width and length of first (driven) patch and so on for three patches, W_f is feed width, S_w and S_l are slot width and length, respectively, in C-band antenna design.

Microwave imaging setup

The microwave imaging setup consists of the proposed broadband reconfigurable antenna as transceiver units, placed two-dimensionally

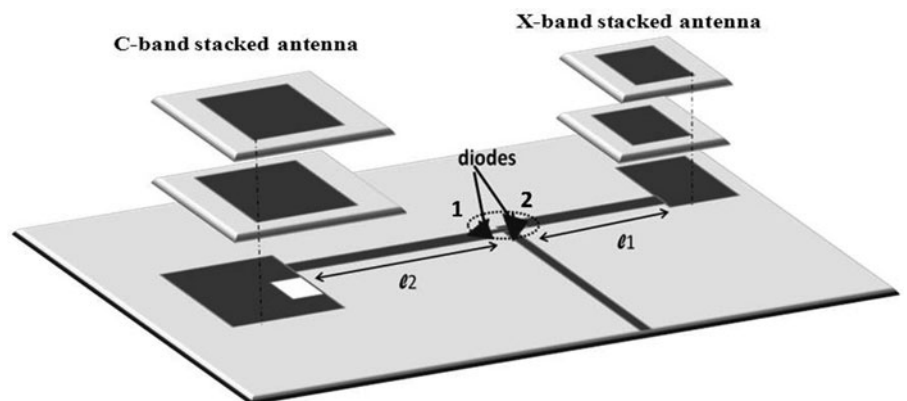


Fig. 1. Reconfigurable antenna/transceiver design.

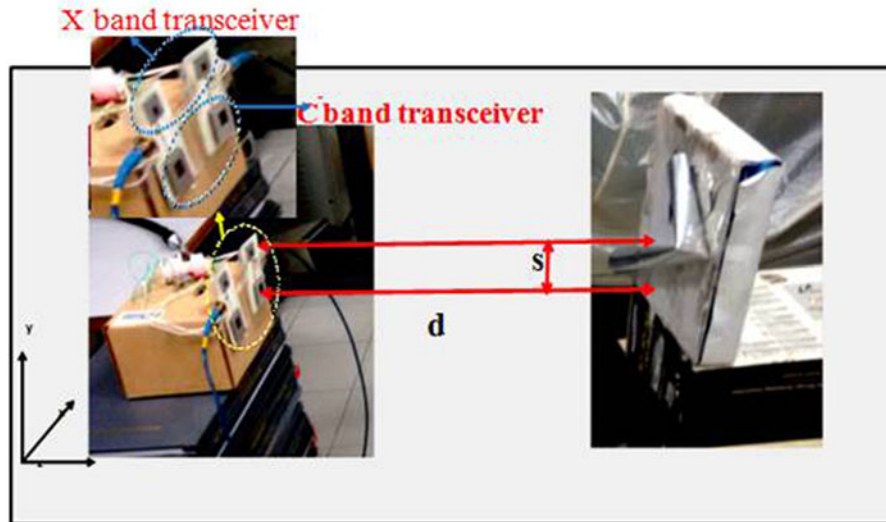


Fig. 3. Measurement setup employing reconfigurable stacked antenna as transceiver.

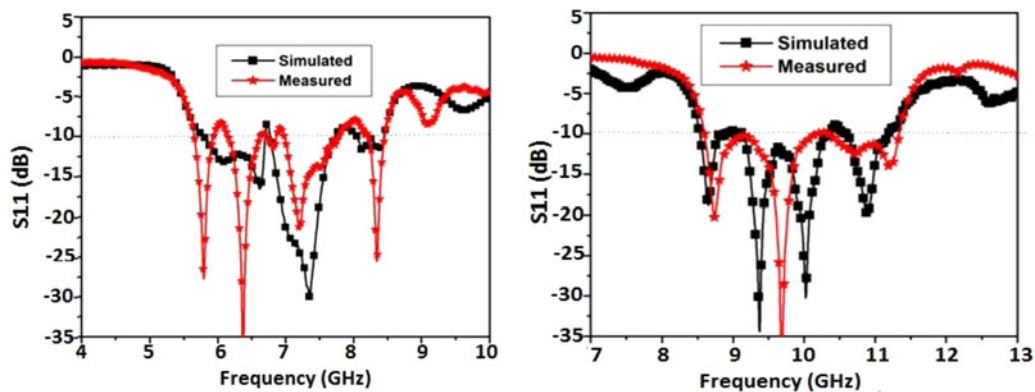


Fig. 4. (a) S_{11} response of reconfigurable antenna for C-band antenna ON, (b) S_{11} response of reconfigurable antenna for X-band antenna ON.

in front of the target under investigation. For laboratory experiments, one transceiver unit is displaced at multiple locations and a vector network analyzer is used as signal generation and data acquisition unit. Here, a bistatic system is employed for 2D scanning of target under test. Microwave imaging measurement setup comprising of reconfigurable stacked antennas as transmitter and receiver (transceiver) is shown in Fig. 3. The reconfigurable antenna is functioning in switching mode, where diode 1 switches ON C-band stacked antenna and diode 2 switches ON X-band stacked antenna in the transceiver. At any instant, C-band antenna is switched ON in both transmitter and receiver, to capture target's spectral information in C-band and similarly it captures spectral information of the target in the X-band, when X-band antenna is switched ON in both the transmitter and receiver units. This reconfigurable transceiver allows collecting target's information in two frequency bands under same environmental conditions for both the states of its operation. The target is kept in the E -plane of both the stacked antennas of the transceiver. The distance between the target and the system's origin is " d ," which is kept equal to 1.1 m in the experiments. The DC supply (batteries) and potentiometer connections are attached to the transceiver support unit. The complete microwave imaging setup is kept in an open lab environment without the use of anechoic chamber or any absorber/s around. The

system ensures rejection of backside clutter as the proposed reconfigurable antenna has unidirectional radiation patterns throughout the operating range. The reflections/scattering due to other nearby objects (in front) in the lab is rejected in the image reconstruction algorithm as described in the next section. Non-planar and irregular-shaped objects have been used as targets. The center of the target is aligned with the center of the transceiver, keeping the environment conditions constant for both the operating states while measuring scattered signal from the target. With this we can obtain the target's spectral information in both the frequency bands through the scattered signal received in each state of operation. This information is then combined in the frequency domain to obtain an equivalent wideband response, which is then processed to obtain target's image.

Image reconstruction

Scattered electric field is calculated and analyzed for multi-point illumination of the target for solving the inverse scattering problem. The investigation domain containing target is scanned two-dimensionally by illuminating the target from different point/angles; conceptually through multiple transceivers, while in experiments by displacing the single transceiver unit at

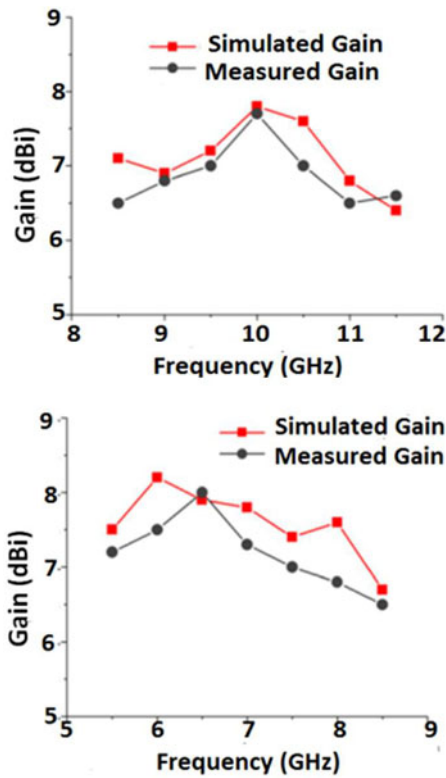


Fig. 5. Measured and simulated gains of C-band and X-band antennae.

multiple locations. The total electric field is given by:

$$E = E_{inc} + E_{scat} \tag{1}$$

In the inverse scattering problem, we find unknown E_{scat} to obtain the target's information, which can be obtained by (2) [26].

$$E_{scat} = j\omega\mu \int_S J_s G(r, r') dr' \tag{2}$$

$$\forall J_s = \tau(r')E(r') \tag{3}$$

Table 1. X-band antenna design parameters [22]

Parameter	Value (mm)	Parameter	Value
W_1	7.5	W_2	7.4 mm
L_1	8	L_2	7.5 mm
Feed width [W_f]	1.1	W_3	7.56 mm
L_3	5	ϵ_{r1}	3.6
h_1	0.508	$\epsilon_{r2}, \epsilon_{r3}$	2.2
h_2, h_3	0.762		

Table 2. C-band antenna design parameters

Parameter	Value (mm)	Parameter	Value
w_1	12	w_3	13.6 mm
L_1	10.89	L_3	12 mm
w_2	13	W_f	1.1 mm
L_2	11	W_s	1.95 mm
Y	7.4	S_l	4.4 mm
h_1	0.508	S_w	2.59 mm
h_2	1.5	ϵ_{r1}	3.6
h_3	2.5	$\epsilon_{r2}, \epsilon_{r3}$	2.2

which essentially is solved for the unknown $\tau(r') = j\omega(\epsilon_{obj} - \epsilon_b)$, called as object function or scattering potential, with the object permittivity ϵ_{obj} and the background permittivity ϵ_b . This is the analytical solution for the unknown target's information. In the present work quick qualitative solution is applied to obtain target's information using the SAR algorithm for image reconstruction. Moreover, the spectral information of the target obtained in two different (but continuous) frequency bands is combined to provide an equivalent wideband response of target in the given scenario. The target placed in the investigation domain is scanned using transceiver in X- and C-band frequency regions. Target's response in both the frequency bands is combined according to (4), where $[S(f_1)]_C$ is the transceiver response in the C-band and $[S(f_2)]_X$ is the transceiver response in the

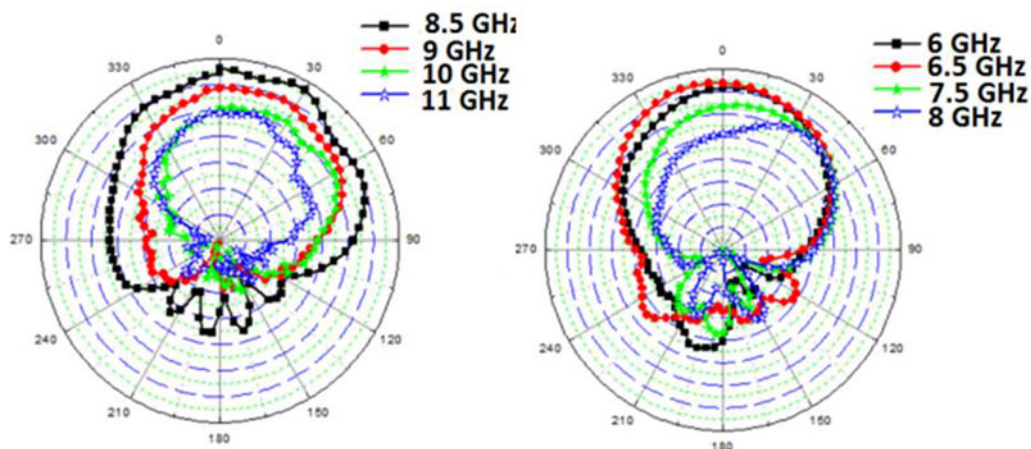


Fig. 6. Measured radiation patterns of reconfigurable stacked microstrip antenna at different frequencies at: (a) C-band antenna ON and (b) X-band antenna ON.

X-band region of operation. This gives wideband spectral information of the target which is processed further to reconstruct the target’s image. Initially, the obtained wideband data (target’s response) are converted into the time-domain form. Furthermore, background subtraction is done where system’s response without the target is obtained in the given scenario, along with considering any scattering from target’s support system. Time gating is applied to the signal to remove the direct signal (from the transmitter to the receiver) and the any other clutter due to surrounding objects:

$$S(f) = [S(f_1)]_C + [S(f_2)]_X \tag{4}$$

$$S(t) = \frac{1}{2\pi} \sum_{-\infty}^{\infty} S(f)e^{j\omega t} \tag{5}$$

$$S_{target}(t) = S(t) - S_{without\ target}(t) \tag{6}$$

$\forall S_{without\ target}(t)$ is obtained similar to $S(t)$, by just removing the target from the given scenario (investigation domain):

$$S_{time-gated}(t) = \sum_{\tau_1}^{\tau_2} S_{target}(t) \tag{7}$$

The range τ_1 - τ_2 needs to be properly chosen/optimized (based on the location of the setup) so as to contain only target’s information and rejecting all the clutter due to nearby objects, as the system is operating in a real open environment. In the present case, measurements are done in a normal lab environment containing several objects near the setup, with many of them being very strong reflectors. Furthermore, this also ensures rejection of high amplitude direct signal, directly reaching the receiver from the transmitter. The averaging operation is performed using Savitzky–Golay filter on the time-domain signal to reduce the effect of noise. Let’s say N signal samples lie in the time-gated signal and a frame length of m is considered for signal smoothing, then signal amplitude at different time instants (samples) is given by:

$$(t_i, A_i); i \in \{1, 2, \dots, m\} \tag{8}$$

These samples are operated with convolution coefficients C_j according to below equation:

$$A_i = \sum_{j=(1-k)/2}^{(k-1)/2} C_j A_{i+1} \tag{9}$$

$$\forall \frac{k-1}{2} \leq i \leq m - \frac{k-1}{2}$$

Here, the convolution coefficients are obtained based on selection of filter order and frame length according to [27]. In the above equations “ k ” is the order of the filter and “ m ” is the frame length. These two parameters need to be optimized properly when working in an open environment for satisfactory noise reduction along with no signal loss. In the present work, after optimization, the values are chosen as: $k = 3$ and $20 < m < 30$ (optimized in case of slight changes in background scenarios). The given target image is obtained using the SAR algorithm for image reconstruction

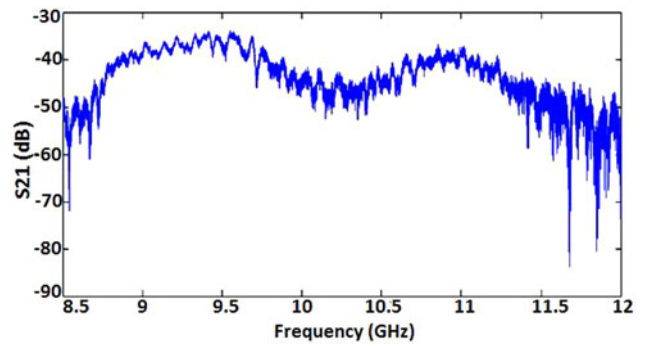


Fig. 7. Response of C-band stacked antenna for bent aluminum rod at 1.1 m.

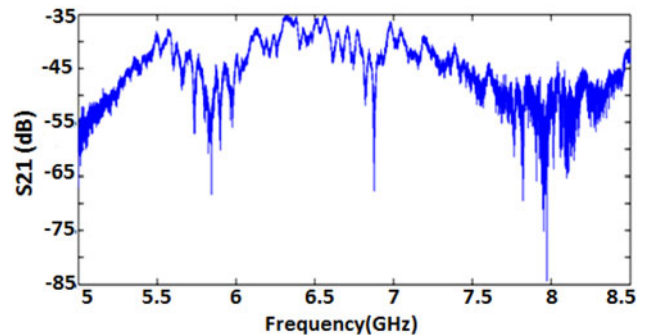


Fig. 8. Response of X-band stacked antenna for bent aluminum rod at 1.1 m.

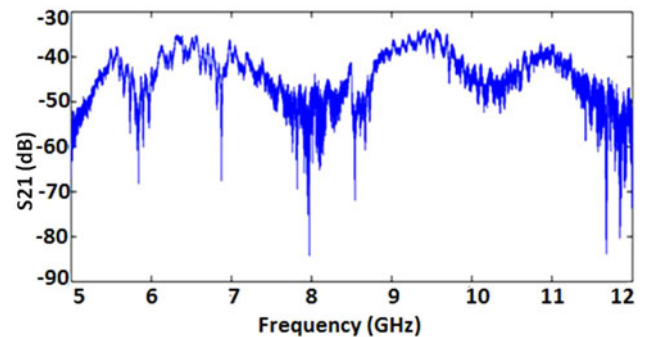


Fig. 9. Response of C- and X-band antennas combined for bent aluminum rod at 1.1 m.

and the algorithm implementation is given by (10) and (11). Let the image matrix be M where initially each matrix cell value is initiated to zero. Then each cell of the matrix $M_j(l, m)$, for j th sensor location and cell location as $x = l$ and $y = m$, is incremented by amplitude A_i (A_i is the signal amplitude at time instant t_i):

$$M_j(l, m) = M_j(l, m) + A_i \tag{10}$$

$$t_i = \tau_1 + (i - 1) \left(\frac{T_2 - \tau_1}{N} \right) \tag{11}$$

$$\forall t_i \approx T(l, m); \quad T(l, m) = 2(D/c)$$

Here, t_i is the value in time vector closest to the time of flight of each cell, i.e. $T(l, m)$, within the limits of 0.1–0.5 ns. Furthermore, D is the distance between j th sensor with location $(x_j, y_j, z = 0)$ and the cell

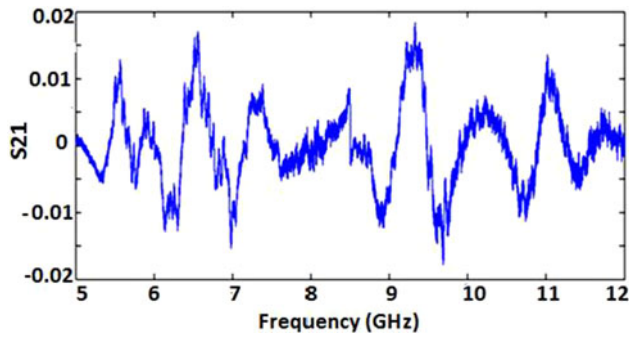


Fig. 10. Response of C- and X-band antennas combined (data in linear form) for bent aluminum rod at 1.1 m.

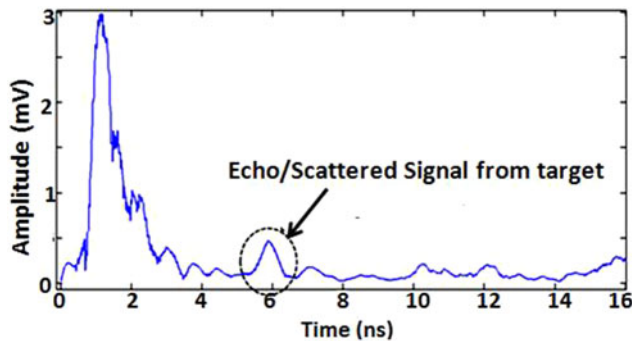


Fig. 11. Time-domain response of combined C- and X-band antennas for bent aluminum rod at 1.1 m.

$(l \times \Delta x, m \times \Delta y, z = d)$; Δx and Δy are the dimensions of each unit cell. Similarly each matrix element is incremented by the amplitude value corresponding to the time-of-flight from the j th transceiver to that element and these amplitude levels keep adding up in each matrix element for $j = 1, 2, \dots$ up to the number of transceivers used for scanning. In our previous work [23], the primitive work of combining information in two operating bands has been carried out by simple image matrix addition in both the bands. However, this method also allows addition of noise/clutter or any error in the image matrix rather than canceling it out. This is, however improved in the proposed novel method of combining frequency domain information, where the background subtraction is done properly over the

combined equivalent broadband frequency range to minimize the effect of noise and any clutter signal due to surroundings.

Results and discussion

The frequency domain responses of X-band antenna and C-band antennas are given in Figs 7 and 8 for the target (bent aluminum rod) kept at 1.1 m. Both of these responses are combined in the frequency domain to get an equivalent broadband response in dB as shown in Fig. 9, while the amplitude variation in linear scale over the wide operating band is shown in Fig. 10. To obtain proper equivalent wideband response using the proposed method, the measurement cables need to be well calibrated over the whole operating range. The combined wideband data are converted into the time domain and are shown in Fig. 11. In the present work, several 3D and irregular-shaped targets are used for experiments to test the imaging algorithm in an open environment. An aluminum sheet has been folded in the cylindrical form and bent to make different target shapes, namely bent rod, U-shaped target, and V-shaped target. All the targets along with their dimensions are depicted in Fig. 12. The imaging setup as mentioned in Section “Microwave imaging setup” and the imaging algorithm mentioned in Section “Image reconstruction” are implemented to obtain target images. The reconstructed target images are shown in Figs 13–15, for bent rod, U-shaped and V-shaped targets, respectively. In the given output images, Figs 13(a) and 13(b) show reconstructed images of bent aluminum rod in the X-band and C-band, respectively. Figure 13(c) shows the reconstructed image of bent rod in the X-band and C-band combined using image matrix addition [20], while Fig. 13(d) shows the reconstructed image of bent rod using the proposed method of combining spectral information obtained in the X- and C-bands. Similarly, Figs 14 and 15 show reconstructed images of U-shaped and V-shaped targets for different cases. As can be observed in Figs 13(a)–15(a), the shape recovery is better in the X-band as higher frequency of operation provides better resolution but it also contains more noise (higher frequency is vulnerable to more environmental noise), as the setup is working in a real open environment. On the other hand, reconstructed images in the C-band shown in Figs 13(b)–15(b) contain lower noise but shape recovery is comparatively poor. Combining these data using image matrix addition shows images obtained are better than those obtained in individual bands as shown in Figs 13(c)–15(c). However, the proposed method of combining spectral information of

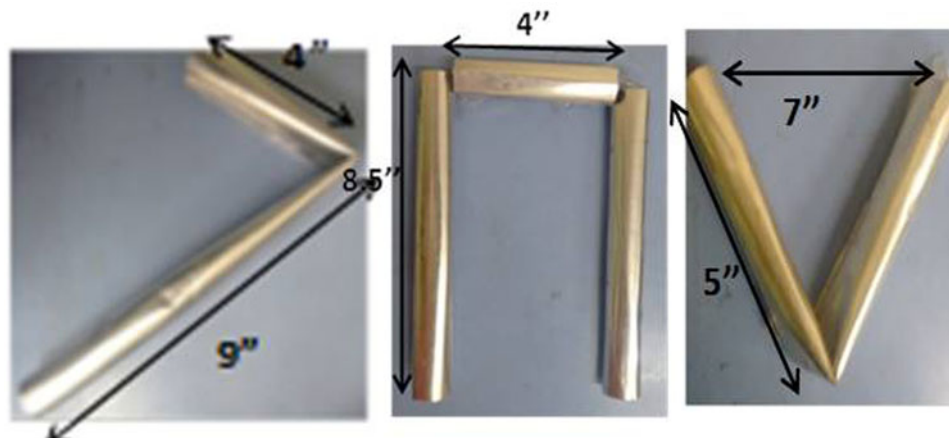


Fig. 12. Non-planar irregular-shaped targets: (a) 3-D bent aluminum rod, (b) U-shaped rod, and (c) V-shaped rod.

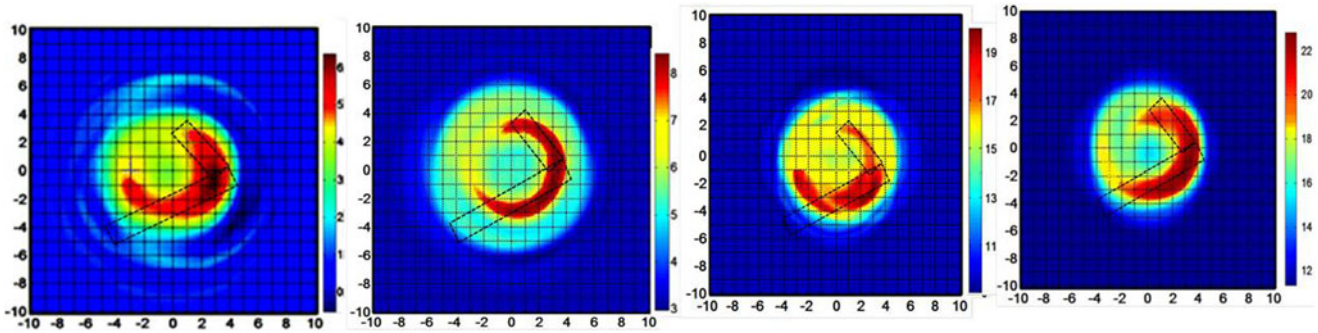


Fig. 13. Image of bent aluminum rod (a) in X-band, (b) in C-band, (c) X- and C-band data combined using image matrix addition, and (d) X- and C-band data combined in the spectral domain by the proposed method.

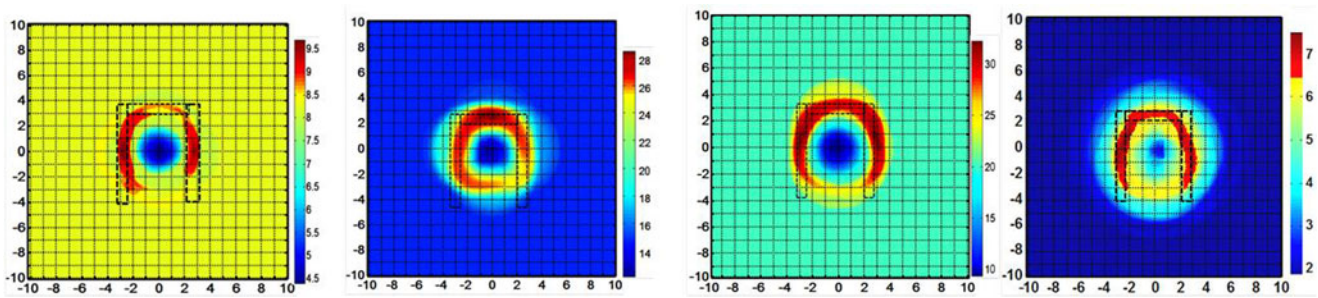


Fig. 14. Image of U-shaped aluminum rod (a) in X-band, (b) in C-band, (c) X- and C-band data combined using image matrix addition, and (d) X- and C-band data combined in the spectral domain by the proposed method.

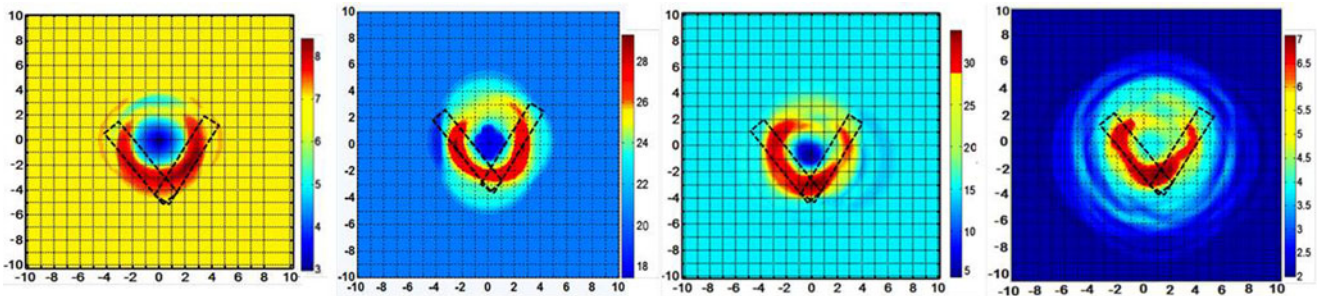


Fig. 15. Image of V-shaped aluminum rod (a) in X-band, (b) in C-band, (c) X- and C-band data combined using image matrix addition, and (d) X- and C-band data combined in the spectral domain by the proposed method.

Table 3. Comparison of microwave imaging measurement systems

Reference	System features	Range	Frequency of operation	Image quality
[14]	Fixed and bulky system, with reflectors, cannot be concealed	0.8 m	0.8–4 GHz	Good
[19]	Fixed and bulky setup	Through-the-wall up to 13 cm	X-band	Only detection
[20]	Bulky setup	Through-the-wall up to 50 cm	0.5–2 GHz	Mostly detection only
[21]	Reflector-backed UWB antenna used as transceiver (non-planar)	11 cm	UWB (2–6.5 GHz)	Average
[22]	Printed (planar) transceivers operating in anechoic chamber	50 cm	C-band	Average
Proposed work	Compact-printed (planar) transceivers operating in real open environment (flexible to implement and can be concealed)	1 m	Multi-band (X-band and C-band)	Average

targets and then processing the image shows clear improvement over the method of matrix addition for adding information in two different bands. These results are depicted in Figs 13(d)–15(d). The aim of the present research is to obtain improved target images in the microwave band to have better range sensitivity as compared to higher frequencies (millimeter waves) in an open environment. Thus, the chosen lower microwave frequency bands have been used here to achieve image reconstruction of unknown irregular-shaped targets in an open environment. The images obtained clearly resemble with the targets, with the further scope of image quality improvement. The comparison of the proposed microwave imaging system with other previous works is presented in Table 3.

Conclusion

The proposed work presents improved image reconstruction of non-planar irregular-shaped metallic targets in open environments using broadband reconfigurable printed transceivers operating in the lower microwave band. The lower microwave band operation ensures better range sensitivity in open environments and microstrip-printed transceiver design keeps the system compact. Furthermore, the concept of switching operating bands in the implemented transceiver to capture target's response provides more spectral information of the target under the same operating conditions. This information when combined in the spectral/frequency domain presents a broadband target's response using printed unidirectional antennas, which itself rejects backside clutter. This specific feature makes it possible to implement the proposed imaging system in an open environment without any need of absorbers. Overall, the proposed compact microwave imaging system can operate in open space and is suitable for inconspicuous microwave imaging systems for metallic object detection. It can find application in hidden wall-mounted systems, hidden system on wall painting or banners, etc., without any need of dedicated chamber having absorbers.

Acknowledgements. The authors acknowledge the support from IIT Delhi in carrying out the experiments and all the support required for the proposed work.

Author contributions. First author has carried out experiments and signal processing for image reconstruction; while both the authors have contributed equally to analyzing data and reaching conclusions, and in writing the paper.

Financial support. There is no funding received for the proposed work from any funding agency, commercial, or not-for-profit sectors.

Conflict of interest. The authors declare that there are no competing interests of financial or personal nature with any of the concerned bodies/persons.

References

1. Amineh RK, Ravan M, Trehan A and Nikolova NK (2011) Near-field microwave imaging based on aperture raster scanning with TEM horn antennas. *IEEE Transactions on Antennas and Propagation* **59**, 928–940.
2. Rezaeieh SA, Zamani A and Abbosh AM (2015) 3-D wideband antenna for head-imaging system with performance verification in brain tumor detection. *IEEE Antennas and Wireless Propagation Letters* **14**, 910–914.
3. Mobashsher AT and Abbosh AM (2016) Performance of directional and omnidirectional antennas in wideband head imaging. *IEEE Antennas and Wireless Propagation Letters* **15**, 1618–1621.
4. Porter E, Kirshin E, Santorelli A, Coates M and Popović M (2013) Time domain multistatic radar system for microwave breast screening. *IEEE Antennas and Wireless Propagation Letters* **12**, 229–232.
5. Porter E, Bahrami H, Santorelli A, Gosselin B, Rusch LA and Popović M (2016) A wearable microwave antenna array for time-domain breast tumor screening. *IEEE Transactions on Medical Imaging* **35**, 1501–1509.
6. Lim HB, Nhung NTT, Li E-P and Thang ND (2008) Confocal microwave imaging for breast cancer detection: delay-multiply-and-sum image reconstruction algorithm. *IEEE Transactions on Biomedical Engineering* **55**, 1697–1704.
7. Fear EC, Sill J and Stuchly MA (2003) Experimental feasibility study of confocal microwave imaging for breast tumor detection. *IEEE Transactions on Microwave Theory and Techniques* **51**, 887–892.
8. Jalilvand M, Li X, Zwirello L and Zwick T (2015) Ultra wideband compact near-field imaging system for breast cancer detection. *IET Microwaves, Antennas and Propagation* **9**, 1009–1014.
9. Geffrin JM, Eyraud C and Litman A (2015) 3-D imaging of a microwave absorber sample from microwave scattered field measurements. *IEEE Antennas and Wireless Propagation Letters* **25**, 472–474.
10. Semenov SY, Bulyshev AE, Abubakar A, Posukh UG, Sizov YE, Souvorov AE, Van den Berg PM and Williams TC (2005) Microwave tomographic imaging of the high dielectric contrast objects using different image reconstruction approaches. *IEEE Transactions on Microwave Theory and Techniques* **53**, 2284–2294.
11. Elboushi A and Sebak A (2014) MMW sensor for hidden targets detection and warning based on reflection/scattering approach. *IEEE Transactions on Antennas and Propagation* **62**, 4890–4894.
12. Eskandari MR, Dehmollaian M and Safian R (2014) Experimental investigation of factorization method as a qualitative approach for near-field microwave imaging. *IEEE Antennas and Wireless Propagation Letters* **13**, 289–292.
13. Malyskin O and Fusco V (2014) Near field enhancement and sub-wavelength imaging using resonantly loaded apertures. *IEEE Transactions on Antennas and Propagation* **62**, 3130–3140.
14. Charvat G, Temme A, Feigin M and Raskar R (2015) Time of flight microwave camera. *Scientific Reports* **5**, Article no. 14709.
15. Bridges JE (1998) Non-invasive system for breast cancer detection. U.S. Patent 5 704 355, Jan. 6, 1998.
16. Hagness SC, Taflove A and Bridges JE (1998) Two-dimensional FDTD analysis of a pulsed microwave confocal system for breast cancer detection: fixed focus and antenna-array sensors. *IEEE Transactions on Biomedical Engineering* **45**, 1470–1479.
17. Li D, Meaney PM and Paulsen KD (2003) Conformal microwave imaging for breast cancer detection. *IEEE Transactions on Microwave Theory and Techniques* **51**, 1179–1186.
18. Meaney PM, Fanning MW, Li D, Poplack SP and Paulsen KD (2000) A clinical prototype for active microwave imaging of the breast. *IEEE Transactions on Microwave Theory and Techniques* **48**, 1841–1853.
19. Paul S, Chugh R and Akhtar MJ (2019) Microwave synthetic aperture radar imaging using SFCW system for buried object detection and security applications. *IEEE International Microwave and RF Conference (IMaRC 2019) INSPEC Accession Number, 19691580*, 1–4.
20. Randazzo A, Ponti C, Feeling A, Estatico C, D'Atanasio P, Pastorino M and Schettini G (2021) A two-step inverse-scattering technique in variable-exponent Lebesgue spaces for through-the-wall microwave imaging: experimental results. *IEEE Transactions on Geoscience and Remote Sensing* **59**, 7189–7200.
21. Shao W, Edalati A, McCollough TR and McCollough WJ (2018) A time-domain measurement system for UWB microwave imaging. *IEEE Transactions on Microwave Theory and Techniques* **66**, 2265–2275.
22. Zhou T, Shen F, Xu K, Tang Z, Wang J, Zhang B, Ye D, Huangfu J, Li C and Ran L (2019) Microwave imaging customized on demand under random field illumination. *IEEE Transactions on Microwave Theory and Techniques* **67**, 1148–1156.
23. Malhotra AA and Basu A (2018) Miniaturised distributed transceivers for far-field microwave imaging. *IEEE International Microwave and RF Conference (IMaRC-2018)*, Dec. 2018, pp. 1–4.
24. Chen WK (2005) *The Electrical Engineering Handbook*. Academic Press, pp. 671–675.
25. Katyal A and Basu A (2017) Analysis and optimisation of broadband stacked microstrip antennas using transmission line model. *IET Microwaves, Antennas and Propagation* **11**, 81–91.
26. Pasterino M (2010) *Microwave Imaging*. John Wiley and Sons. Inc. Publications.
27. Schafer RW (2011) What is a Savitzky – Golay filter?. Lecture Notes. *IEEE Signal Processing Magazine*.



Ankita Malhotra (earlier known as Ankita Katyal) was born on September 17, 1987. She received her B.E. in electronics and communication engineering from KEC Dwarahat in 2009 and her M.Tech. in 2011 from the College of Technology G.B.P.U.A.T. Pantnagar. She received her Ph.D. in RF and microwave from IIT Delhi in 2017. Currently she is working as an assistant professor in Electronics and Telecommunication

Department in Rajiv Gandhi Institute of Technology, Mumbai. Her areas of interest include antenna design and analysis, microwave imaging and its applications.



Ananjan Basu was born on August 12, 1969. He received his B.Tech. in electrical engineering and his M.Tech. in communication and radar engineering from the Indian Institute of Technology Delhi (I.I.T. Delhi), in 1991 and 1993, respectively, and his Ph.D. in electrical engineering from the University of California at Los Angeles (UCLA), in 1998. He has been with the Centre for Applied Research in Electronics, I.I.T. Delhi, as an assistant professor (2000–2005), associate professor (2005–2012), and professor (since 2012). His specialization is in microwave and millimeter-wave component design and characterization.